

# Unraveling the topological charge of optical force in a solid dielectric material

Xiang Xi<sup>1</sup>, Jingwen Ma<sup>1</sup>, Zhong-Hao Zhou<sup>2,3</sup>, Xin-Xin Hu<sup>2,3</sup>, Yuan Chen<sup>2,3</sup>, Chang-Ling Zou<sup>2,3\*</sup>, Chun-Hua Dong<sup>2,3\*</sup> & Xiankai Sun<sup>1\*</sup>

<sup>1</sup>Department of Electronic Engineering, The Chinese University of Hong Kong, Shatin, New Territories, Hong Kong

<sup>2</sup>CAS Key Laboratory of Quantum Information, University of Science and Technology of China, Hefei, Anhui 230026, China

<sup>3</sup>CAS Center for Excellence in Quantum Information and Quantum Physics, University of Science and Technology of China, Hefei, Anhui 230026, China

\*Corresponding author. Email: [clzou321@ustc.edu.cn](mailto:clzou321@ustc.edu.cn) (C.L.Z.); [chunhua@ustc.edu.cn](mailto:chunhua@ustc.edu.cn) (C.H.D.); [xksun@cuhk.edu.hk](mailto:xksun@cuhk.edu.hk) (X.S.)

The force exerted by electromagnetic fields is of fundamental importance in broad sciences and applications<sup>1-3</sup>, but its exact formulation inside materials is still controversial and unclear<sup>4-6</sup>. The textbook-accepted formulation of electromagnetic force was proposed by Lorentz in the 19th century, but its validity has been challenged due to incompatibility with the special relativity and momentum conservation<sup>7,8</sup>. The Einstein–Laub formulation, which can reconcile those conflicts, was suggested as an alternative to the Lorentz formulation<sup>8-10</sup>. However, intense debates on the exact force inside materials are still going on due to lack of experimental evidences. Here, we report the first experimental investigation of topological charge of optical force inside a solid dielectric material, aiming to distinguish the two formulations. The experiments show that the optical force exerted by a Gaussian beam has components with the topological charge of both 2 and 0, which cannot be supported solely by the Lorentz or the Einstein–Laub formulation. Instead, we found a modified Helmholtz theory could explain our experimental results. The unraveled topological charge of optical force will not only contribute to the ultimate determination of the correct force formulation inside materials, but also update the fundamental working principle for many science and engineering branches involving electromagnetic forces.

The Lorentz (LO) law of electromagnetic force is regarded as one of the foundations of classical electrodynamics. However, this century-old physical law has been in crisis<sup>11</sup>. In the 1960s, Shockley pointed out that the LO law contradicts the universal momentum conservation in certain systems involving magnetic materials<sup>7,12,13</sup>. More recently, the LO law was also found to be incompatible with the special relativity, as it predicts different results in different reference frames<sup>8</sup>. These problems of the LO law could be avoided by introducing an additional hidden momentum of electromagnetic field in magnetic materials<sup>7,8</sup>. However, there still lack wide agreements on this issue because the hidden momentum is experimentally unobservable with current technique. At the same time, another formulation originally proposed by Einstein and Laub (EL) has also been widely used and was suggested as an alternative of the electromagnetic force formulation<sup>4,8-10,14-21</sup>, as it complies with both the special relativity and universal conservation laws without needing the hidden momentum<sup>8,22,23</sup>. The EL formulation is also consistent with the Maxwell's equations, and agrees with the existing measurement results of the total force or torque that support the LO formulation<sup>19,24</sup>. Their equivalence on the total force or torque measurements leads to most of the existing experiments<sup>4-6</sup> failing to distinguish these two formulations. To date, the debates on the LO and EL formulations are still going on because rigorous experimental investigations on distinguishing them are still absent.

The underlying difference between the LO and EL formulations lies in their different descriptions of the quantum nature of materials and electromagnetic fields: the LO formulation treats the electric and magnetic dipoles inside a material as distributions of ordinary charges and currents, while the EL formulation treats the electric and magnetic dipoles as two individual constituents that are distinct from ordinary charges and currents<sup>17,19</sup>. Due to the different treatments, the LO force in a nonmagnetic dielectric material has the form  $\mathbf{F}_{\text{LO}} = (-\nabla \cdot \mathbf{P})\mathbf{E} + \partial\mathbf{P}/\partial t \times \mathbf{B}$ , while the EL force has the form  $\mathbf{F}_{\text{EL}} = (\mathbf{P} \cdot \nabla)\mathbf{E} + \partial\mathbf{P}/\partial t \times \mathbf{B}$ , with  $\mathbf{E}$  the electric field,  $\mathbf{B}$  the magnetic induction, and  $\mathbf{P} = \epsilon_0(\epsilon_r - 1)\mathbf{E}$  the polarization (Supplementary Sec. 2).  $\epsilon_0$  and  $\epsilon_r$  are the vacuum permittivity and the relative permittivity of the material, respectively. Note that the hidden momentum problem can be avoided naturally in nonmagnetic dielectric materials, inside which the hidden momentum is always zero. It was recently discovered that although these two formulations predict the same total force on an object, they actually produce different force distributions inside a dielectric material<sup>19,21</sup>. This feature can be harnessed to distinguish the two

formulations in experiments, and can also be utilized to reveal the quantum nature of materials. However, the predicted differences are microscopic and exist only inside a material, which were thought to be too weak to be detected.

Here, we experimentally investigated the optical force distribution inside a solid dielectric material by using an optomechanical approach with ultrahigh detection sensitivity. For a linearly polarized optical beam of Gaussian profile propagating in a dielectric medium (Fig. 1a), the LO formulation predicts a force distribution tending to stretch (compress) the medium along (perpendicular to) the light polarization direction (Fig. 1b). By contrast, the EL formulation predicts a force distribution tending to compress the medium radially inward (Fig. 1c)<sup>19,21</sup>. More specifically, in the cylindrical coordinates, the force density in the LO formulation has a form of  $\mathbf{F}_{\text{LO}}(r, \theta, z) = [f_r^{\text{LO}}(r)\cos 2(\theta + \phi), -f_r^{\text{LO}}(r)\sin 2(\theta + \phi), 0]$ , and the force density in the EL formulation is  $\mathbf{F}_{\text{EL}}(r, \theta, z) = [f_r^{\text{EL}}(r), 0, 0]$ , with  $\phi$  the polarization angle of the optical beam. The functions  $f_r^{\text{LO}}(r)$  and  $f_r^{\text{EL}}(r)$  are related to the optical fields and vary only along the radial direction (Supplementary Sec. 2). Their different azimuthal properties determine that the optical force density mode possesses the topological charge (or angular momentum quantum number)  $C = 2$  by the LO formulation (Fig. 1b) or  $C = 0$  by the EL formulation (Fig. 1c). Therefore, one can distinguish these two formulations by experimentally measuring the topological charge of the optical force instead of the absolute mechanical displacement. The absolute mechanical displacement is intrinsically extremely weak and can easily be masked by noises, but the topological charge of the force is robust due to the topologically protected symmetry of the force and can unambiguously be determined as an integer.

As schematically illustrated in Fig. 1a, we employed an optical-fiber-based system to identify the topological charge of optical force in the fiber. A critical property of optical force is that the LO force with  $C = 2$  is strongly dependent on the optical polarization angle  $\phi$  while the EL force with  $C = 0$  is independent of  $\phi$ . Therefore, the oscillating amplitude of a mechanical mode actuated by forces of different  $C$  would respond differently when the optical polarization angle  $\phi$  varies. In our system, the optical force was exerted by an optical field propagating in the core of a single-mode optical fiber (Fig. 1a). The intensity of the optical field was sinusoidally modulated to actuate the mechanical modes (Fig. 1d) of the optical fiber. The amplitude response of a mechanical mode

to the optical force is proportional to the spatial overlap integral  $\iiint \mathbf{F}(\mathbf{r}) \cdot \mathbf{u}(\mathbf{r}) d\mathbf{r}$ , where  $\mathbf{F}(\mathbf{r})$  is the force density distribution and  $\mathbf{u}(\mathbf{r})$  is the displacement field of the mechanical mode. The mechanical field  $\mathbf{u}(r, \theta, z) = [U_m(r)\cos n(\theta + \phi_m), V_m(r)\sin n(\theta + \phi_m), W_m(r)\cos n(\theta + \phi_m)]$  of the mechanical mode also contains an angular mode number  $n$ , where  $U_m(r)$ ,  $V_m(r)$ , and  $W_m(r)$  have complicated expressions involving the Bessel functions,  $\phi_m$  is the angle of symmetry axis of the mechanical mode and can be set as  $0^\circ$  for convenience (Supplementary Sec. 1). According to the spatial overlap integral, the mechanical mode with angular mode number  $n$  can only respond selectively to the force with  $C = n$  in ideal case. Since the topological charge  $C$  can be 2 or 0, both the mechanical modes with  $n = 2$  (wine-glass mode, Fig. 1d) and  $n = 0$  (breathing mode, Fig. 1d) were examined. Due to the resonant enhancement effect, these mechanical modes could have amplified mechanical motion in response to the force oscillating at the mechanical eigenfrequencies. The intensities of the actuated mechanical modes were obtained with ultrahigh sensitivity from optomechanical transduction by using an ultrahigh- $Q$  optical whispering-gallery mode traveling in the circumference of the transverse plane, which was supported by the slightly fused cladding of the optical fiber<sup>25</sup> (Fig. 1a; Supplementary Sec. 1).

In practice, the device fiber could not be perfectly cylindrical. By taking the geometry imperfection into consideration, the amplitude of mechanical mode with angular mode number  $n$  actuated by the force with topological charge  $C$  is proportional to an integral  $\int \cos[C(\theta + \phi)] \{ \cos[n(\theta + \phi_m)] + \sum_l \sigma_l^{(n)} \cos[l(\theta + \phi_m)] \} d\theta$  (Supplementary Sec. 3), where  $\sum_l \sigma_l^{(n)} \cos[l(\theta + \phi_m)]$  accounts for the small geometry-imperfection-induced mechanical modal distortion in the angular direction ( $\sigma_l^{(n)} \ll 1$ ). Based on the integral, we summarized three criteria for determining the topological charge of the optical force inside the dielectric material:

- (I) For a single pump beam with polarization angle  $\phi$ , the intensity of mechanical mode actuated by a force with  $C = 2$  is proportional to  $|\cos(2\phi)|^2$ , while that by a force with  $C = 0$  is polarization-independent (Supplementary Sec. 3.2 and Fig. S6c).
- (II) For dual pump beams with polarization angles  $\phi_1$  and  $\phi_2$ , the intensity of mechanical mode actuated by two synchronously modulated forces with  $C = 2$  is proportional to  $|\cos(\phi_1 + \phi_2) \cos(\phi_1 - \phi_2)|^2$ , while that by forces with  $C = 0$  is polarization-independent (Supplementary Sec. 3.3 and Fig. S6d).

(III) For dual orthogonally polarized pump beams with a RF modulation phase difference  $\Delta\phi_{\text{RF}}$ , the intensity of mechanical mode actuated by forces with  $C = 2$  is proportional to  $|\sin(\Delta\phi_{\text{RF}}/2)|^2$ , while that by forces with  $C = 0$  is proportional to  $|\cos(\Delta\phi_{\text{RF}}/2)|^2$  (Supplementary Sec. 3.4 and Fig. S6e).

To experimentally examine the topological charge of optical force under the three criteria, we fabricated a bottle-like microstructure on a standard single-mode optical fiber (Fig. 2; Supplementary Sec. 1). We slightly fused the cladding of the fiber to create the two necks of the bottle-like microstructure (Fig. 2a), whose diameters range from 100 to 120  $\mu\text{m}$  for different samples tested in the experiment (Supplementary Fig. S1). Such bottle-like device configuration forms optical and mechanical energy potentials that can support high-quality optical probe modes and mechanical modes (Figs. 1a and 1d; Supplementary Sec. 1). The pump light beam that exerts an optical force to actuate the mechanical modes propagates in the fiber core (Fig. 2b), with the beam shape preserving a quasi-Gaussian profile after fabricating the bottle-like microstructure (Figs. 2c and S2). The pump light is also experimentally confirmed to be quasi-linearly polarized (Supplementary Sec. 4.4). Such quasi-linearly polarized Gaussian pump light beam well satisfies the critical experimental requirements for the theoretical analysis about force density distribution and the three criteria to examine the force formulations above (Supplementary Secs. 3 and 6).

The topological charge of the optical force was experimentally investigated by measuring the intensity of the wine-glass mode ( $n = 2$ ) according to Criteria I and II. First, we measured the response of mechanical intensity to the polarization angle of a single pump beam. It was found that the mechanical intensity follows the pump beam's polarization angle  $\phi$  with a dependence of  $|\cos(2\phi)|^2$ , with  $>20$  dB extinction ratio (Fig. 3a). Next, we applied two pump beams and measured the response of the same mechanical mode to the two pump beams' polarization angles  $\phi_1$  and  $\phi_2$ . It was found that the mechanical intensity follows  $|\cos(\phi_1 + \phi_2) \cos(\phi_1 - \phi_2)|^2$  (Fig. 3b), with  $>20$  dB extinction ratio. When  $\phi_2$  is fixed at  $0^\circ$ , the measured mechanical intensity follows a dependence of  $|\cos\phi_1|^4$  (Fig. 3c). Specifically, for two orthogonally polarized pump beams ( $\phi_1 = 90^\circ, \phi_2 = 0^\circ$ ), the measured mechanical intensity is much weaker than that actuated by a single pump beam ( $\phi = 0^\circ$  or  $90^\circ$ ), indicating that the forces of two orthogonally polarized pump beams

cancel each other out (Figs. 3d–3f). According to Criteria I and II, these results indicate the existence of force component with  $C = 2$ .

To further investigate the topological charge of optical force, we also measured the actuation results of the breathing mode ( $n = 0$ ) with the same experimental configuration. With a single pump beam, the mechanical intensity does not vary with the polarization angle (Fig. 4a). In addition, the mechanical intensity also remains constant under actuation by dual pump beams with different polarization angles (Fig. 4b). According to Criteria I and II, these results indicate that the optical force also has a component with  $C = 0$ .

Next, the topological charge of optical force was also investigated under the condition in Criterion III, where the wine-glass mode ( $n = 2$ ) and the breathing mode ( $n = 0$ ) each were actuated by two orthogonally polarized pump beams modulated at the same RF frequency but with a constant phase difference  $\Delta\phi_{\text{RF}}$ . Figure 5a shows the measured mechanical intensity of the wine-glass mode ( $n = 2$ ) as a function of  $\Delta\phi_{\text{RF}}$ , which follows the dependence of  $|\sin(\Delta\phi_{\text{RF}}/2)|^2$  and confirms the existence of force component with  $C = 2$ . On the other hand, the mechanical intensity of the breathing mode ( $n = 0$ ) follows  $\Delta\phi_{\text{RF}}$  with a dependence of  $|\cos(\Delta\phi_{\text{RF}}/2)|^2$  (Fig. 5b), which confirms the existence of force component with  $C = 0$ .

The above experimental results indicate that the optical force by a linearly polarized Gaussian beam in a solid dielectric material has components with a topological charge of both  $C = 2$  and  $C = 0$ . Such results are also confirmed to be valid even when slight distortion in the optical and mechanical modes introduced during the device fabrication process is considered in the experiments (Supplementary Sec. 6). It is interesting to note that the force component with topological charge  $C$  was confirmed selectively from the actuation results of the mechanical mode with  $n = C$ , due to the satisfaction of phase matching. Nonetheless, a small portion of crosstalk also exists, yielding actuation of the mechanical modes with  $n \neq C$ . This is actually attributed to geometry imperfection of the optical fiber used in the experiment. By taking this factor into account, we numerically simulated the actuated mechanical intensities and compared them with the measured results, concluding that the ratio between the force components with  $C = 2$  and  $C = 0$  is between 1:3 and 1:1 (Supplementary Sec. 7). Therefore, these two force components are

comparable in magnitude. Since the LO and EL formulations each predict an optical force with a unique topological charge ( $C = 2$  or  $C = 0$ ), neither of them can explain our experimental results.

Although the unraveled topological charge of optical force contradicts the predictions of both the LO and EL formulations, our results are consistent with previous experimental observation by Ashkin and Dziedzic in 1973<sup>26</sup>—a bulge appeared on water surface at the spot where a focused laser beam entered, which was ever taken as an evidence supporting the EL formulation<sup>20,21</sup>. According to our experimental results, such a bulge can appear as long as the angularly symmetric compressive force component with  $C = 0$  exists. Because of the fluidic nature of liquids, it is challenging to measure the angularly antisymmetric force component with  $C = 2$ , and thus it has never been identified before. It should also be noted that the Hakim–Higham experiment in 1962<sup>27</sup> was believed to support the Helmholtz force over that by Einstein and Laub. Actually, the Hakim–Higham experiment only showed the strength of electric pressure along the  $y$  axis in their setup. Such a one-dimensional scalar measurement is not enough to determine the distribution and topological charge of electromagnetic force inside a medium. Additionally, those experiments based on liquids<sup>4,5,15,28,29</sup> are mostly phenomenological with many spurious effects<sup>4,21</sup>. They do not provide much microscopic information about the force distribution, so they cannot shed much light on determining the correct force formulation inside a material. By contrast, our experiment based on a lossless solid dielectric avoids most of the ambiguous effects encountered previously, and our findings reveal for the first time the microscopic properties of optical force inside a material. We expect that these results will not only generate long-term impact on understanding of the light–material interactions, but also update the fundamental working principle for many applications in science and engineering branches involving optical forces.

Although the experiments were planned based on the force distributions inside a material predicted by the LO and EL formulations, the experimentally unraveled topological charge can be used to examine any other related theories. Besides the LO and EL formulations, there are also many other electromagnetic force theories<sup>4–6</sup> to describe the force. The force density distribution of a Gaussian beam in an optical fiber predicted by these existing theories can also have a topological charge  $C = 2$  or  $C = 0$ . Exhaustive scrutiny of all the force formulations, however, is beyond the scope of this work. Here, we found a modified Helmholtz theory by combining the Lorentz formulation with the electrostrictive force<sup>30,31</sup> could account for the existence of both force

components with  $C = 2$  and  $C = 0$ , which possibly explains our experimental results (Supplementary Sec. 8). This modified Helmholtz theory can be also consistent with the results of the Ashkin–Dziedzic and Hakim–Higham experiments. On the other hand, since the EL formulation has already included the electrostrictive interaction<sup>4,24</sup>, it may require other types of modification to explain the experimental results. We believe that the topological charge of optical force unraveled in this work will serve as a crucial step in the ultimate determination of the correct electromagnetic force formulation inside material in the future.



## References

1. Ashkin, A. Acceleration and trapping of particles by radiation pressure. *Phys. Rev. Lett.* **24**, 156–159 (1970).
2. Chu, S., Hollberg, L., Bjorkholm, J. E., Cable, A. & Ashkin, A. Three-dimensional viscous confinement and cooling of atoms by resonance radiation pressure. *Phys. Rev. Lett.* **55**, 48–51 (1985).
3. Dholakia, K. & Čížmár, T. Shaping the future of manipulation. *Nat. Photonics* **5**, 335–342 (2011).
4. Brevik, I. Experiments in phenomenological electrodynamics and the electromagnetic energy-momentum tensor. *Phys. Rep.* **52**, 133–201 (1979).
5. Brevik, I. Radiation forces and the Abraham–Minkowski problem. *Mod. Phys. Lett. A* **33**, 1830006 (2018).
6. Milonni, P. W. & Boyd, R. W. Momentum of light in a dielectric medium. *Adv. Opt. Photon.* **2**, 519–553 (2010).
7. Shockley, W. & James, R. P. "Try simplest cases" discovery of "hidden momentum" forces on "magnetic currents". *Phys. Rev. Lett.* **18**, 876–879 (1967).
8. Mansuripur, M. Trouble with the Lorentz law of force: incompatibility with special relativity and momentum conservation. *Phys. Rev. Lett.* **108**, 193901 (2012).
9. Einstein, A. & Laub, J. About the ponderomotor forces exerted on resting bodies in the electromagnetic field. *Annalen der Physik* **331**, 541–550 (1908).
10. Einstein, A. & Laub, J. About the basic electromagnetic equations for moving bodies. *Annalen der Physik* **331**, 532–540 (1908).
11. Cho, A. Textbook electrodynamics may contradict relativity. *Science* **336**, 404–404 (2012).
12. Shockley, W. "Hidden linear momentum" related to the  $\vec{\alpha} \cdot \vec{E}$  term for a Dirac-electron wave packet in an electric field. *Phys. Rev. Lett.* **20**, 343–346 (1968).
13. Coleman, S. & Van Vleck, J. H. Origin of "hidden momentum forces" on magnets. *Phys. Rev.* **171**, 1370–1375 (1968).
14. Fano, R. M., Chu, L. J. & Adler, R. B. *Electromagnetic Fields, Energy, and Forces* (Wiley, New York, 1960).
15. Gordon, J. P. Radiation forces and momenta in dielectric media. *Phys. Rev. A* **8**, 14–21 (1973).
16. Walker, G. B. & Lahoz, D. G. Experimental observation of Abraham force in a dielectric. *Nature* **253**, 339–340 (1975).
17. Vaidman, L. Torque and force on a magnetic dipole. *Am. J. Phys.* **58**, 978–983 (1990).
18. Loudon, R. Theory of the forces exerted by Laguerre-Gaussian light beams on dielectrics. *Phys. Rev. A* **68**, 013806 (2003).
19. Barnett, S. M. & Rodney, L. On the electromagnetic force on a dielectric medium. *J. Phys. B* **39**, S671 (2006).
20. Loudon, R. Radiation pressure and momentum in dielectrics. *Fortschr. Phys.* **52**, 1134–1140 (2004).
21. Mansuripur, M., Zakharian, A. R. & Wright, E. M. Electromagnetic-force distribution inside matter. *Phys. Rev. A* **88**, 023826 (2013).
22. Mansuripur, M. Electromagnetic force and torque in ponderable media. *Opt. Express* **16**, 14821–14835 (2008).
23. Mansuripur, M. Radiation pressure and the linear momentum of the electromagnetic field in magnetic media. *Opt. Express* **15**, 13502–13518 (2007).

24. Mansuripur, M. Force, torque, linear momentum, and angular momentum in classical electrodynamics. *Appl. Phys. A* **123**, 653 (2017).
25. Asano, M. *et al.* Observation of optomechanical coupling in a microbottle resonator. *Laser Photon. Rev.* **10**, 603–611 (2016).
26. Ashkin, A. & Dziedzic, J. M. Radiation pressure on a free liquid surface. *Phys. Rev. Lett.* **30**, 139–142 (1973).
27. Astrath, N. G. C., Malacarne, L. C., Baesso, M. L., Lukasiewicz, G. V. B. & Bialkowski, S. E. Unravelling the effects of radiation forces in water. *Nat. Commun.* **5**, 4363 (2014).
28. Li, Z., Weilong, S., Nan, P. & Ulf, L. Experimental evidence for Abraham pressure of light. *New J. Phys.* **17**, 053035 (2015).
29. Hakim, S. S. & Higham, J. B. An experimental determination of the excess pressure produced in a liquid dielectric by an electric field. *Proc. Phys. Soc.* **80**, 190–198 (1962).
30. Boyd, R. W. *Nonlinear Optics*. (Elsevier, 2003).
31. Rakich, P. T., Davids, P. & Wang, Z. Tailoring optical forces in waveguides through radiation pressure and electrostrictive forces. *Opt. Express* **18**, 14439–14453 (2010).

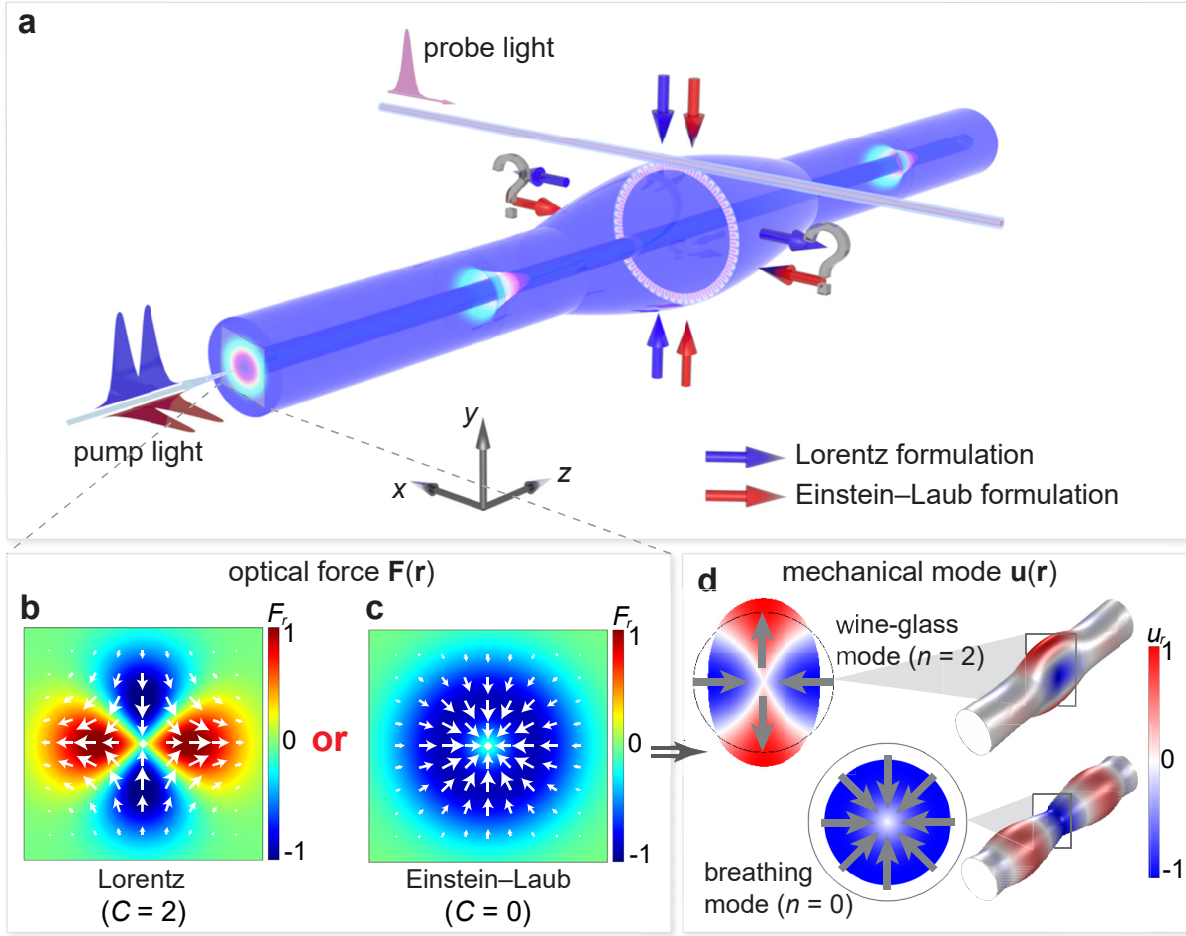


**Fig. 1 | Optical force distribution inside a solid dielectric.** **a**, Schematic of the measurement setup. A linearly polarized Gaussian pump beam is launched into a single-mode fiber. The force exerted by the optical field deforms the optical fiber in the transverse direction. The deformation is detected by a probe field through an ultrahigh- $Q$  optical whispering-gallery mode supported in the transverse plane of a bottle-like microcavity formed by the slightly fused cladding of the optical fiber. The blue and red arrows denote the force directions inside the optical fiber by a  $x$ -polarized pump beam in the LO and EL formulations respectively, which are opposite in the  $x$  direction. **b**, **c**, Calculated force distributions of the pump beam according to the LO and EL formulations.  $F_r$  is the force component in the radial direction, where the outward direction is defined as positive. The LO force has a topological charge  $C = 2$ , while the EL force has a topological charge  $C = 0$ . **d**, Profiles of the mechanical wine-glass mode ( $n = 2$ ) and breathing mode ( $n = 0$ ). The arrows indicate the directions of mechanical displacement.

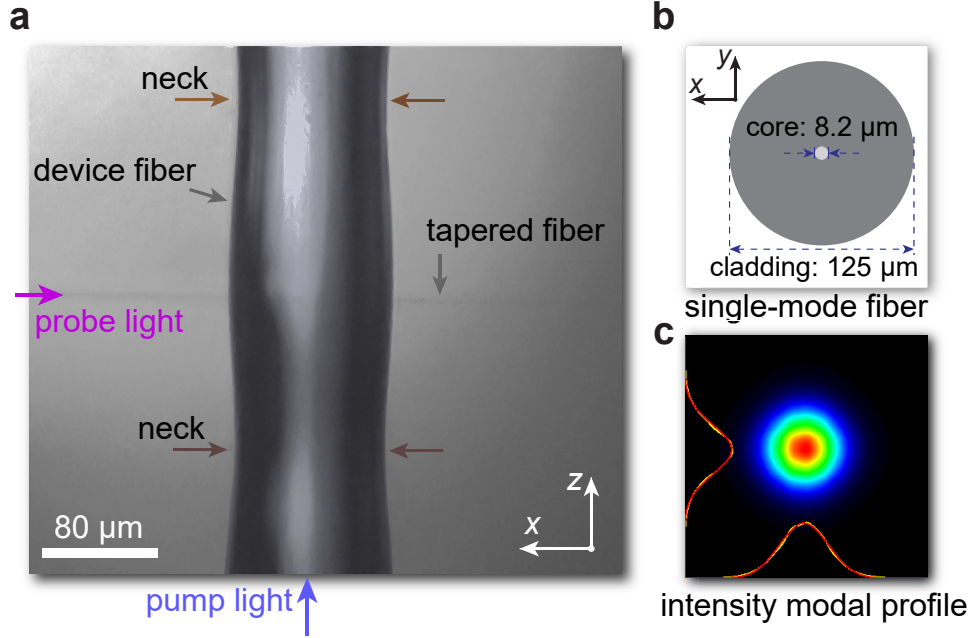


**Fig. 2 | Device image and experimental configuration.** **a**, Optical microscope image of the device fiber (showing the part of the bottle-like microstructure) and the tapered fiber in the experimental setup. The pump light beam propagates in the core of the device fiber. The probe light beam is sent through the tapered fiber to be coupled into and out of a whispering-gallery cavity mode supported in the transverse plane of the bottle-like microstructure. The two necks on the device fiber were created by slight laser fusing on a standard single-mode fiber (Supplementary Information). **b**, Illustration of cross section of the standard single-mode fiber with labeled dimensions. **c**, Optical intensity distribution measured from a cut facet of the fiber at the device region, where the yellow and red lines represent the measured and Gaussian-fitted profiles, respectively.

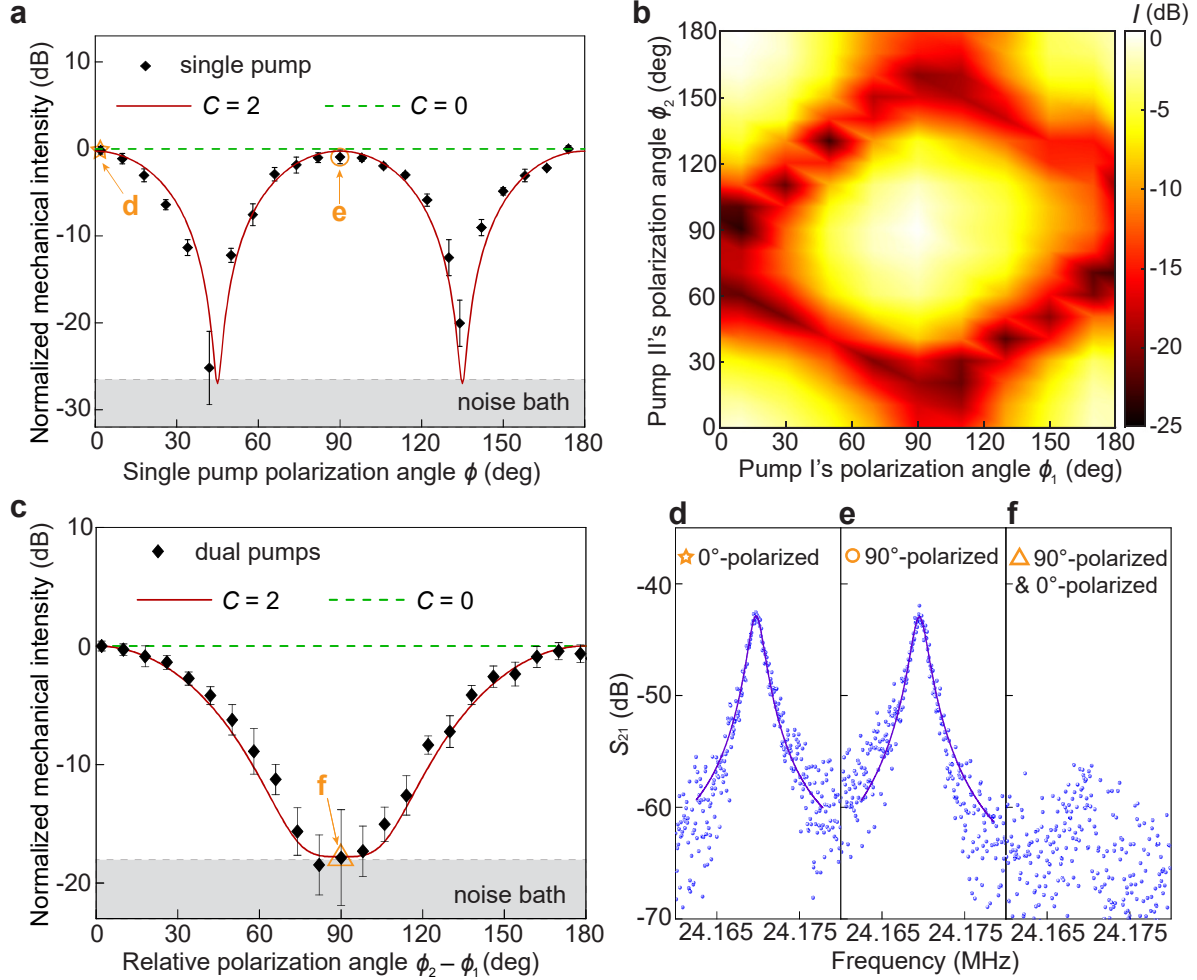


**Fig. 3 | Dependence of actuated intensity of the wine-glass mode ( $n = 2$ ) on polarization angle(s) of pump beam(s).** **a**, Measured mechanical intensity as a function of the polarization angle of a single pump beam. **b**, Measured mechanical intensity as a function of the polarization angles of dual pump beams. **c**, Measured mechanical intensity as a function of the relative polarization angle  $\phi_2 - \phi_1$  of two pump beams, where  $\phi_1$  is fixed at  $0^\circ$ . **d**, **e**, **f**, Measured  $S_{21}$  spectra showing the relative intensity of the actuated wine-glass mode. The mode in **d** and **e** was actuated by a single pump beam polarized at  $0^\circ$  and  $90^\circ$ , respectively; the mode in **f** was actuated by two pump beams polarized at  $0^\circ$  and  $90^\circ$ . In **a** and **c**, the red solid and green dashed lines plot the theoretically predicted results for force with  $C = 2$  and  $C = 0$ , respectively, where the bath noise extracted from the experimental data has been included. The mechanical intensity is normalized to its maximum. The error bars represent one standard deviation from the mean.

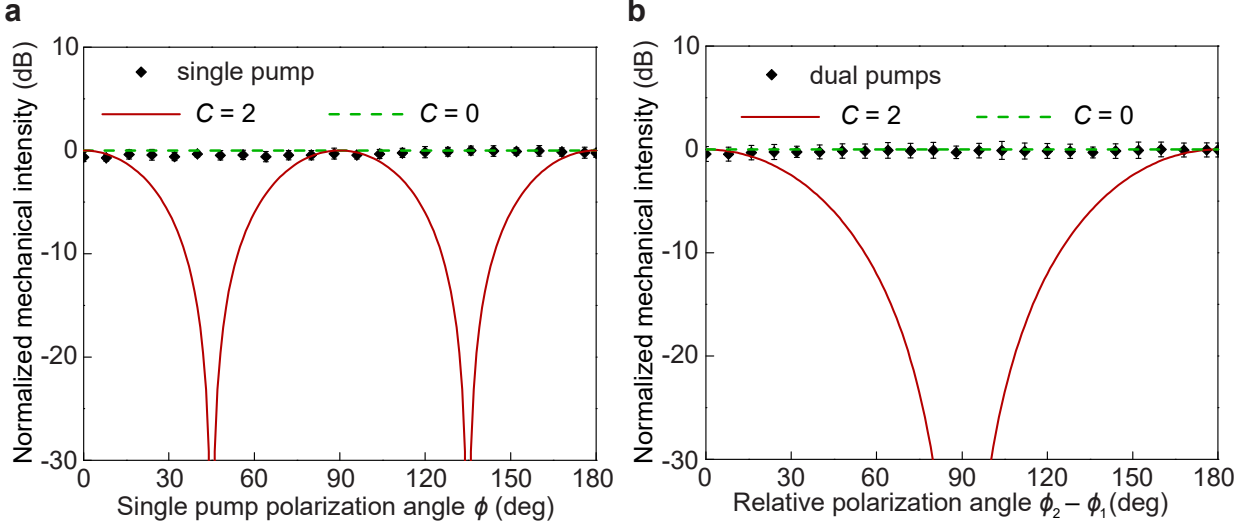


**Fig. 4 | Dependence of actuated intensity of the breathing mode ( $n = 0$ ) on polarization angle(s) of pump beam(s).** **a**, Measured mechanical intensity as a function of the polarization angle of a single pump beam. **b**, Measured mechanical intensity as a function of the relative polarization angle  $\phi_2 - \phi_1$  of dual pump beams, where  $\phi_1$  is fixed at  $0^\circ$ . The error bars represent one standard deviation from the mean.

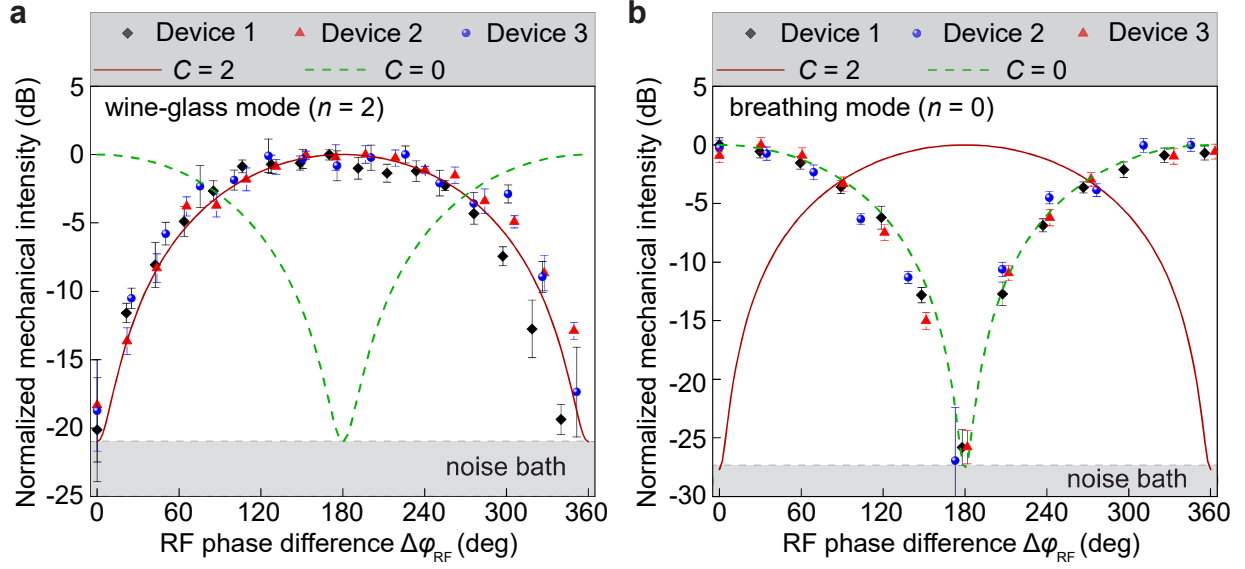


**Fig. 5 | Dependence of actuated intensity of mechanical modes on the RF modulation phase difference  $\Delta\phi_{\text{RF}}$  of two orthogonally polarized pump beams. a, b, Measured mechanical intensity of the wine-glass mode ( $n = 2$ ) (a) and the breathing mode ( $n = 0$ ) (b) as a function of the RF modulation phase difference  $\Delta\phi_{\text{RF}}$  of the two pump beams. The error bars represent one standard deviation from the mean.**